Mariner IX Optical Navigation Using Mars Lit Limb

NAVIN JERATH* AND HIROSHI OHTAKAY†
Jet Propulsion Laboratory, Pasadena, Calif.

Optical spacecraft navigation data, i.e., the lit limb TV image of Mars, acquired during the approach phase of the Mariner IX spacecraft to Mars, has been successfully demonstrated to augment the radio spacecraft tracking data. Accurate in-flight calibration of the TV instrument and the scan platform was performed by referencing stars and planets. Simulated real-time processing and the detailed postflight analyses of the onboard optical data have shown that planet limb data is an important data source in a far-encounter period for which other types of onboard optical measurements, e.g., natural satellite(s) of the target planet with star background, may not be available.

Nomenclature

a	= semimajor axis of fit ellipse
B	= magnitude of $\bar{B}$ vector
c	= focus of fit ellipse
l, p	= limb data point in scan line, pixel directions
l_o, p_o	= image center location in scan line, pixel directions
t_i	= time of the ith observation
T	= time of flight
T_i	= difference between T and t_i
V_∞	= velocity on the approach asymptotes
$\Delta\bar{B}\cdot\bar{R}, \Delta\bar{B}\cdot\bar{T}$	= components of $\Delta\bar{B}$ in the $\bar{R}$, $\bar{T}$ directions
$SMAA, SMIA$	= semimajor and semiminor axes of the B-plane one-sigma uncertainty ellipse
Var( )	= variance of argument
δ( )	= perturbation
θ_i	= angle between velocity vector and direction to Mars at time t_i
ξ	= limb observation noise
ϕ	= optical observable
ψ	= inclination of Mars spin axis relative to TV coordinate system

Introduction

OPTICAL navigation has been demonstrated to be an effective method for interplanetary navigation.[1,2] Various optical data types[3] which can be obtained from science and engineering instruments normally aboard such spacecraft can be used. TV cameras are used to view planets or satellites and stars for celestial references. This paper presents the results of post-flight optical navigation investigations using data on the lit limb of Mars obtained from the Mariner IX mission.

The sources of data were the digitally transmitted TV picture along with supporting engineering data. Processing of the raw data included the elimination of systematic errors occurring in the onboard measurement system and the reduction of the TV lit limb image data to image center location data. These measurements were used to determine the relative location of the spacecraft with respect to the target planet.

Presented as Paper 73-251 at the AIAA 11th Aerospace Sciences Meeting, Washington, D.C., January 10–12, 1973; submitted February 26, 1973; revision received January 25, 1974. This paper presents the results of one phase of research carried out at the Jet Propulsion Laboratory, California Institute of Technology, under Contract NAS 7-100, NASA. The authors wish to acknowledge the efforts of the optical navigation team in support of this analysis, and JPL's Image Processing Laboratory for providing photographs and reseau data.

Index categories: Spacecraft Navigation, Guidance, and Flight-Path Control Systems; Aerospace Technology Utilization; Navigation, Control, and Guidance Theory.

* Research Engineer, Mission Analysis Division.

† Senior Engineer, Guidance and Control Division.

The navigation analysis deals with two aspects of the Mars limb data. The first is an evaluation of the performance that could have resulted had the processing been performed in real time for computing the Mars Orbit Insertion (MOI) maneuver, and the second is its sensitivity to Mars ephemeris errors and the amount of radio tracking data. The investigation indicates that though the estimate obtained from the real-time simulation would have been within Mariner IX mission accuracy requirements, the uncertainty of the estimate is large. Performance has been found to be somewhat sensitive to the amount of radio tracking data but not to Mars ephemeris error.

Onboard Measurement Systems

Instruments onboard the Mariner spacecraft which were utilized to obtain the data included the narrow- and wide-angle science TV cameras and the attitude control sensors. TV cameras were mounted on a scan platform provided with two degrees of freedom. The $1.1° \times 1.4°$ and $11° \times 14°$ field-of-view vidicons with 9.6 mm × 12.5 mm selenium targets were electronically scanned in 700 lines with 832 picture elements (pixels) per line. Continuous video intensity level was sampled and digitized to 9 bits (512 levels) prior to transmission to Earth. The attitude control subsystem provided spacecraft stabilization and orientation. Its celestial sensors, i.e., Sun sensors and star (Canopus) sensor, produced pitch, yaw, and roll position signals. The attitude control signals, together with the scan platform gimbal position data, were transmitted to the ground station through the engineering telemetry channels.

TV picture-taking sequences were commanded and supervised by the onboard computer. Video data of about 30 TV frames for one picture-taking sequence were temporarily stored on magnetic tape. The magnetic tape playback for data transmission to the Earth was commanded when the Goldstone antenna station was in a favorable position for direct communication with the Mariner IX spacecraft.

Inflight Calibration of Onboard Measurement Instruments

Calibrations of the onboard measurement instruments were subject to change due to factors such as mechanical shock experienced during spacecraft launch and midcourse maneuvers as well as gravity and electromagnetic environmental changes. This necessitated inflight instrumental calibration to be performed prior to spacecraft guidance and navigation data acquisition.

Calibration of the TV camera geometric distortion was necessary to establish undistorted image direction relative to the TV coordinate system. This was performed by utilizing both reseau

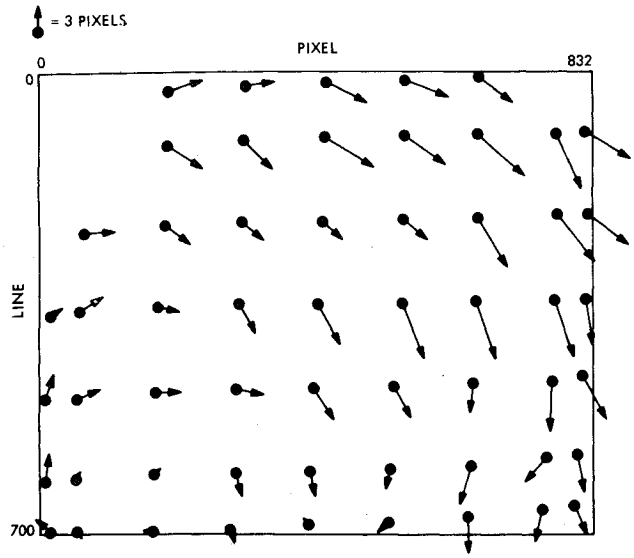

Fig. 1 Change in observed reseau location of narrow-angle TV.

marks etched on the vidicon target and celestial references (stars) with known directions. The former allows calibration of electromagnetic geometric distortion arising inside the vidicon, while the latter is used to calibrate optical distortion in the camera optics combined with electromagnetic distortion. Since ground calibration of the TV cameras revealed practically no optical geometric distortion for the narrow-angle TV camera and small optical distortion (<2.5 pixels), for the wide-angle TV camera, no attempt was made during flight to estimate optical distortion parameters.

Electromagnetic geometric distortion was calibrated by fitting 63 and 111 reseau images observed in the narrow and wide angle TV calibration pictures, respectively, to the analytical geometric distortion model.[4] Electromagnetic geometric distortion was calibrated to the accuracy of 0.5 (1σ) pixels and 0.7 (1σ) pixels in the line and pixel directions, respectively, for the narrow- and wide-angle TV cameras. Changes of observed reseau locations in narrow-angle TV pictures between preflight and inflight calibrations (Fig. 1) were caused by the absence of Earth's magnetic field and possibly by a slight displacement of TV beam deflection coils.

Calibration of the scan platform subsystem was necessary to establish the true scan platform orientation (hence TV image direction) relative to the spacecraft. The scan platform errors were characterized by systematic errors such as gimbal mounting errors, gimbal axis misalignments, and TV instrument mounting offsets placed on the scan platform. Attitude control sensor signal values were needed to define the spacecraft attitude relative to the celestial references. Systematic errors of the telemetered attitude control sensor signals are characterized by sensor null offsets and scale factor errors. Inflight calibration of the scan platform subsystem and attitude control sensors was performed by referencing to the orientation of the narrow-angle TV imaged stars and planets whose locations were known a priori. Mechanical misalignments of the wide-angle TV were calibrated with respect to the narrow angle TV. Two sequences of 31 pictures aimed at star clusters, single stars, Mars, and Saturn, provided a good set of data for calibration of the scan platform subsystem and attitude control sensors. The star-referenced inflight calibration[6] determined the scan platform subsystem and attitude control errors to a total accuracy of 0.005° (1σ) about the TV line of sight (LOS) and 0.020° in cone and cross-cone axes for the narrow-angle TV camera and 0.015° (1σ) and 0.17° (1σ), respectively, for the wide-angle TV camera.

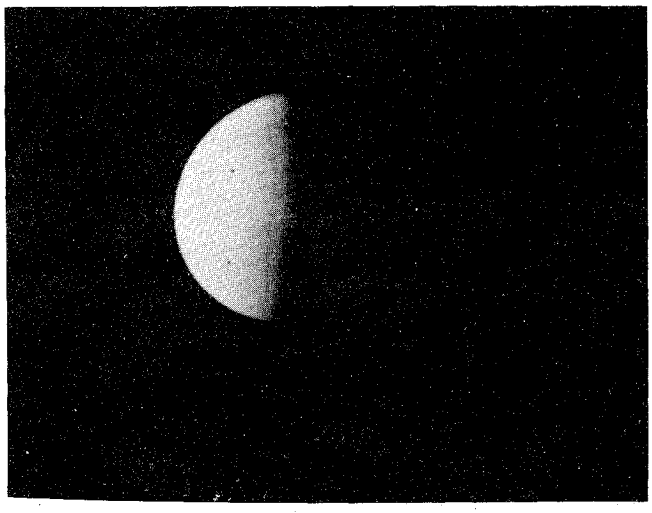

Fig. 2 Typical Mars lit limb TV picture.

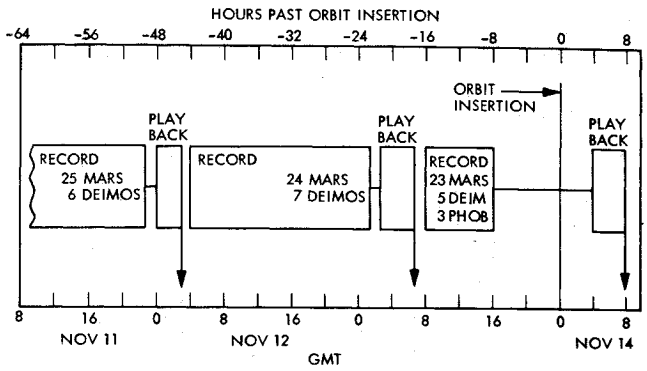

Fig. 3 Approach picture sequence.

Limb Data Algorithm and Processing

During the two Mars calibration sequences which took place five and four days before Mars encounter (abbreviated as E-5d and E-4d, respectively), 22 narrow-angle TV pictures which contained Mars lit limb images (Fig. 2) were taken. Wide-angle TV pictures of Mars during the Mars calibration sequences were not processed because of poor angular resolution. During POS (preorbit Science) I, II, and III sequences which started from E-3.1d, E-1.9d, and E-0.7d, respectively, 36 narrow-angle TV pictures and four wide-angle TV pictures were selected for lit limb data processing where POS-I and II pictures were available in real time before MOI (see Fig. 3). Towards the end of POS-II and throughout POS-III sequences, the Mars images taken by the narrow-angle TV were so large that only a small portion of the lit limb was visible; hence such frames were not processed.

Raw TV data of Mars' image was first processed to determine the lit limb in the TV coordinate system. The limb-finding algorithm searched the digital video data TV scan line by scan line. That is, the limb search started from a point off the planet image and continued onto the limb. The first of three adjacent pixels, all having video intensity levels exceeding a predetermined threshold level, was selected as the location of lit limb on that line. The requirement for three adjacent pixels eliminated the detection of false limb point caused by one or two pixel-bit error noise (Fig. 4). Typical lit limb structure imaged by the narrow-angle camera (Fig. 4) indicates a relatively sharp decline in brightness near the equator and a gradual decline at the pole regions. The transition region between the dark background and the apparent limb ranged from 15 km to 25 km wide near the equator, and 25 km to 30 km wide at the pole regions.

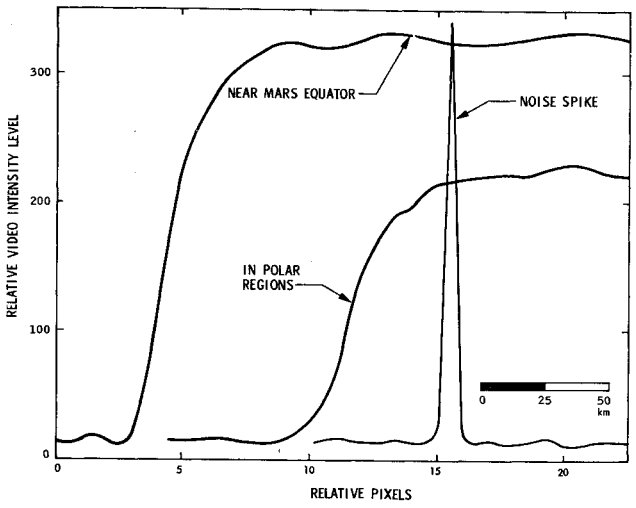

Fig. 4 Mars limb image structures.

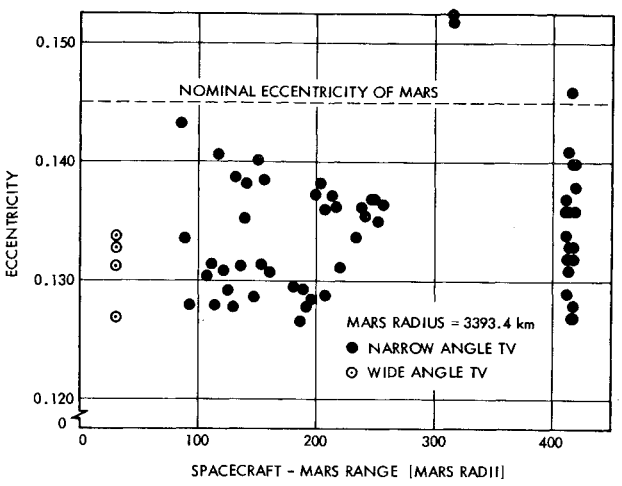

Fig. 6 Observed Mars shape parameter.

To interpret the imaged Mars lit limb, Mars was assumed to be an ellipsoid with small eccentricity (=0.145). Since the Mariner spacecraft approached Mars only about 20° off the equatorial plane of Mars, TV image of Mars can be reasonably well modeled by an ellipse, with the center of the ellipse being coincident with the center of the ellipsoidal planet body.

The apparent lit limb data was processed for TV distortion rectification based upon the inflight calibration of the TV instruments. Then, a minimum-variance estimation algorithm was used to identify the true image shape, size, and orientation as well as the image center location, which rendered significant uncertainty. The observable equation used in the estimation process to fit the distortion corrected lit limb data was the following function[7]:

$$\phi = \left(1 - \frac{c^2}{a^2}\right)x^2 + y^2 - a^2 + c^2 + \xi \tag{1}$$

$$\begin{bmatrix} x \\ y \end{bmatrix} = \begin{bmatrix} \cos\psi & -\sin\psi \\ -\sin\psi & -\cos\psi \end{bmatrix} \begin{bmatrix} p - p_o \\ l - l_o \end{bmatrix}$$

In this equation, the observable, ϕ, takes a zero value if ξ, the observation noise, is zero.

The identified size of the planet (Fig. 5) has a larger ($\sim$100 km) value than the known mean equatorial radius (3397.2 km) determined by the *S*-band occultation experiment.[8] Similarly, the identified shape parameter of the planet (Fig. 6) is smaller than the known value ($e = 0.145$) by about 3%. That is, the Mars images were somewhat larger and more circular than expected. These results indicate that the lit limb of the imaged planet does not represent the Martian surface: they are reasoned to have been caused by reflection from a light-scattering surface from the Martian atmosphere together with the combined effects of image blooming and unmodeled bending of the electron beam in the vicinity of the bright image of the vidicon. They may also have been caused by the limb-darkening effect at the polar regions and lightening near the south polar cap, marked albedo change near the lit limb, atmospheric acitivites, i.e., the dust storm which prevailed in the Martian atmosphere throughout the approach phase, and the spectral response characteristics of the TV camera subsystem, including the particular filter (minus blue) used for the narrow-angle TV throughout the mission.

The limb fit residuals, which are a measure of the observation data noise after a successful limb parameter estimation process, were evaluated for each scan line containing a limb measurement (Fig. 7) with the units of (pixel).[2] The observation data noise had been caused by quantization in picking discrete limb points, uncalibrated geometric distortion of the TV, residual limb image from the previous picture (triggering a false limb data), and limb model approximation error. To interpret the limb residual statistics with nearly zero-mean and a standard deviation of several tens of (pixel),[2] the residual random process is mapped onto an equivalent random process along the limb image in the TV coordinate system. From Eq. (1) we obtain

$$\text{Var}(\delta\phi) = c_p^2\,\text{Var}(\delta p) + c_l^2\,\text{Var}(\delta l) \tag{2}$$

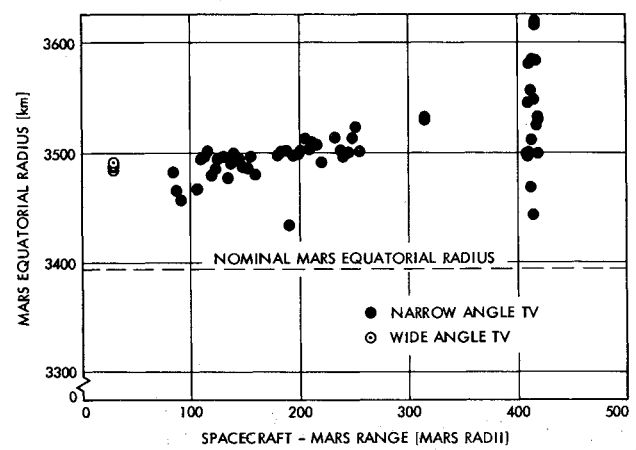

Fig. 5 Observed Mars mean equatorial radius.

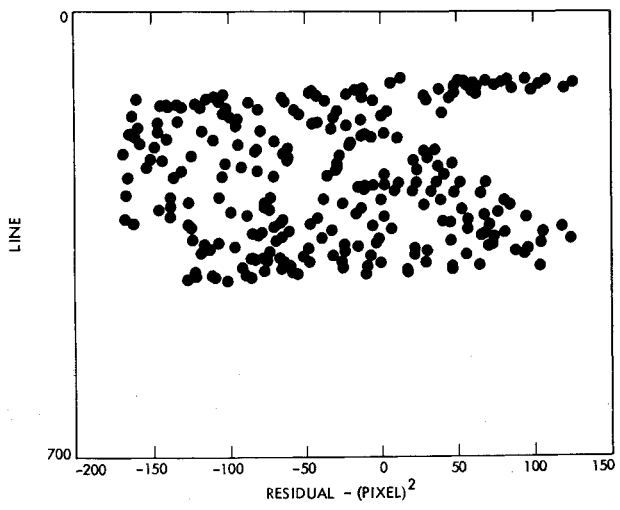

Fig. 7 Mars lit limb fit residuals.

where

$$c_p^2 = 4\left[-\left(1-\frac{c^2}{a^2}\right)x\sin\psi + y\cos\psi\right]^2$$

$$c_l^2 = 4\left[\left(1-\frac{c^2}{a^2}\right)x\sin\psi + y\cos\psi\right]^2$$

If it is assumed that the observation noise affects equally in line and pixel directions, Eq. (2) can be rewritten as

$$\mathrm{Var}(\delta p) = \mathrm{Var}(\delta l) = [\mathrm{Var}(\delta\phi)/c_l^2 + c_p^2] \quad (3)$$

or for typical values for the known parameters relations, e.g., $c/a = 0.145$ and $x^2+y^2 \approx a^2$, Eq. (3) is approximated by

$$\mathrm{Var}^{1/2}(\delta p) = \mathrm{Var}^{1/2}(\delta l) \approx \mathrm{Var}^{1/2}(\delta\phi)/2a \quad (4)$$

Equation (4) typically took a value of 0.3 pixels, reasonably well coinciding with the limb quantization error statistics (a uniform distribution over a pixel). Equation (4) was also evaluated for each TV frame and was mapped along the planet limb by using the equation of collinearity (Fig. 8). Similar results from the Mariner VI and VII missions are shown in the same figure for comparison. The improvements by a factor of at least two are owing to the accurate inflight calibration of the TV instruments and the scan platform.

Optical Data Errors and Approach Trajectory Analysis

Optical navigation observables were defined as the image locations (pixel and line numbers) of the center of Mars. Optical data errors are classified as model and instrument errors.

Model errors include Mars ephemeris, shape, and gravity field errors. Instrument errors include TV distortions, TV pointing errors, image center-finding errors, and random measurement errors. The center-finding errors are modeled as a combination of a constant error proportional to the image size, along with random errors. These random errors are a few pixels in magnitude. The target parameters used for accuracy analysis are the B plane parameters.[3]

Optical observations involve the measurement of angles between the target planet and a fixed reference direction. Such angular measurements suffer from the inability to determine the velocity (V_∞) of the spacecraft as well as accurate time of flight. To illustrate this, consider a spacecraft moving on trajectory no. 1 (Fig. 9). Let θ_1 and θ_2 represent two angular measurements of the direction between the reference direction (which we have for simplicity assumed to be along V_∞) and the target planet. Then the observable equation is $\tan\theta_i = B/V_\infty T_i$.

Two perfect observations θ_1 and θ_2 enable one to determine the time of flight. However, since the observation history for any trajectory parallel to trajectory no. 1 will have the same time of flight as the true trajectory, all trajectories parallel to the true

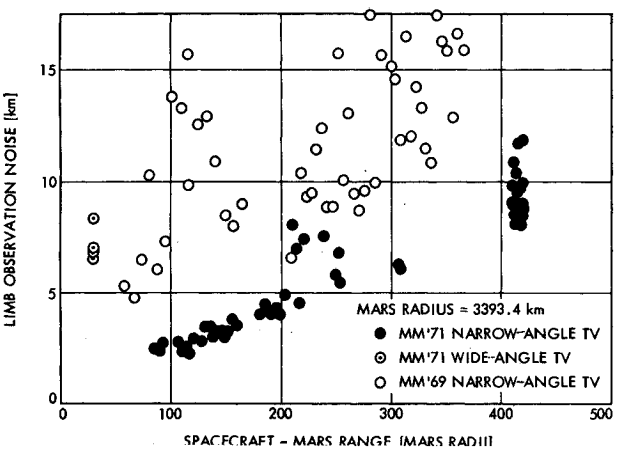

Fig. 8 Mars lit limb observation noise statistics.

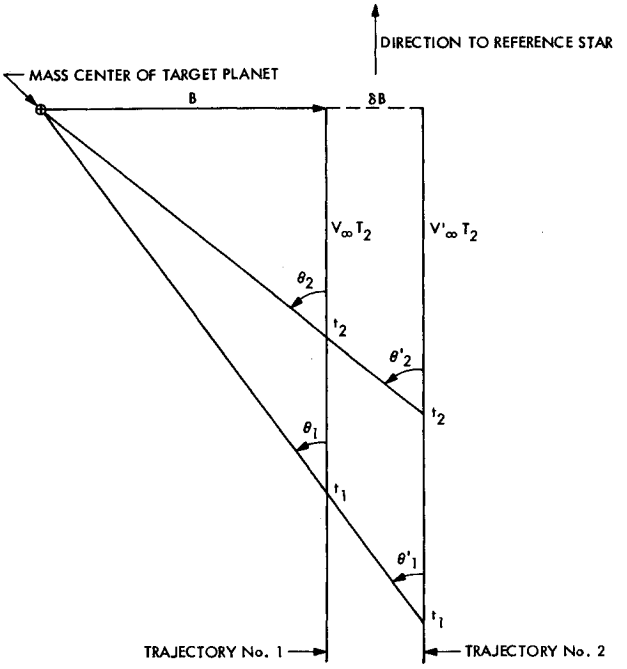

Fig. 9 Approach trajectory geometry.

trajectory are indistinguishable using these angular measurements. The determination of V_∞ then requires further information on the flight history. For small angles θ, the limiting accuracy for B with perfect observation is then given by $\delta B/B = \delta V_\infty/V_\infty$.

Information on V_∞ is obtained from planetary bending of the approach trajectory. For computing the MOI maneuver, Doppler data would have to be used, since planetary bending of the spacecraft trajectory sets in only when the planet is in very close proximity.

So far, it has been assumed that the angular measurements θ_i are perfect. However, various sources of errors arise in these measurements, some of the most common of which are the camera-pointing and center-finding errors which lead to inaccuracies in the calculated time of flight.

For small observation angles θ_1 and θ_2, $T = (t_2\theta_2 - t_1\theta_1)/(\theta_2-\theta_1)$ and

$$\delta T = \frac{(t_2-t_1)(\theta_2\,\delta\theta_1 - \theta_1\,\delta\theta_2)}{(\theta_2-\theta_1)^2} \quad (5)$$

Assuming independent observations, the standard deviation σ_T of T becomes

$$\sigma_T = [V_\infty T_1 T_2(T_1^2+T_2^2)^{1/2}/B(T_1-T_2)]\sigma_\theta \quad (6)$$

Equation (6) indicates that the uncertainty in the time of flight is very sensitive to the uncertainty in the pointing angle when the spacecraft is far from the planet. It is seen that the error is minimized for smaller V_∞ which decreases the range at which the observations are taken, and by larger B values which increase parallax.

Simulated Real-Time Results

The TV data available in real time for computing the MOI maneuver, namely the data through PO II, was processed using as a priori the best trajectory available at that time. The trajectory was based on radio tracking data processed through E-13 hours. The picture data from Mars calibration sequences I and II and POS sequences I and II were used for the analysis. Of these pictures, the Mars calibration II pictures (at E-4 days) were dropped because of the very large data residuals due to large pointing errors.

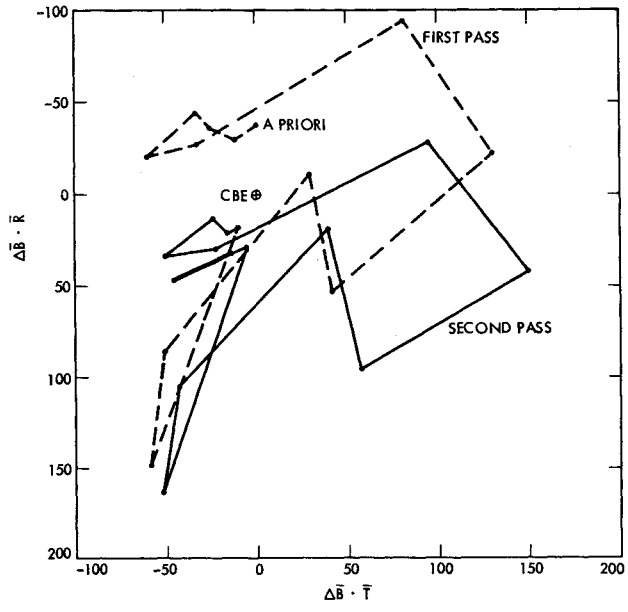

Fig. 10 Simulated real-time results.

Figure 10 shows the *B*-plane solution history of the trajectory estimate obtained by processing the optical data. The parameters estimated were the spacecraft Cartesian state at epoch, TV pointing biases and errors, and image center-finding errors. The origin in the figure is at the current best estimate (CBE).[9] The a priori shown for the optical data arc was the a posteriori estimate from a short radio data arc (5 days) through E-13 hours. The estimate stabilized only towards the last few pictures. Two iterations were performed, indicated by the dashed and full lines, respectively, with the last two points on the full line representing the estimates obtained from POS III data. These were played back after orbit insertion (Fig. 3) so were not available in real time. The final estimate at the end of POS II data

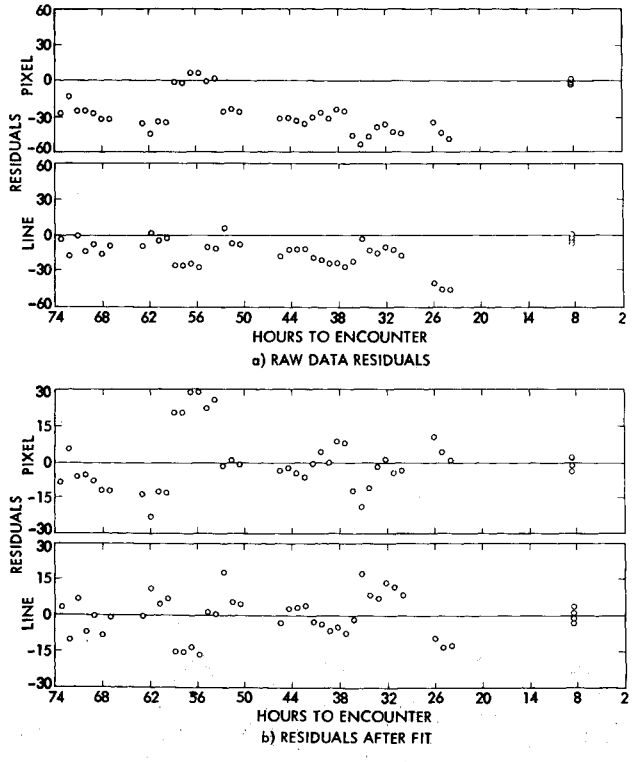

Fig. 11 POS data residuals.

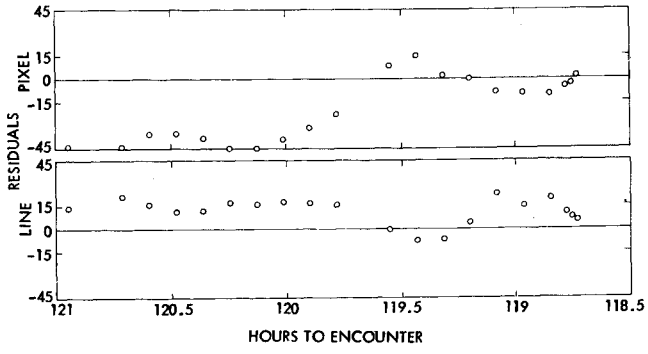

Fig. 12 Mars-calibration sequence raw data residuals.

had an SMAA of 70 km. This was within 25 km of the CBE, well within Mariner IX mission navigation requirements (50 km) for MOI.

Figure 11a shows the pre-estimation data residuals in the pixel and line directions for the POS data. Figure 11b shows the residuals after the solved for pointing biases and trajectory error have been removed. The magnitude of the pointing biases estimated agreed with scan calibration results.[6] The center-finding errors, modeled here as being proportional to the image size, appeared to be very small. The pointing errors in the raw data are not random.

The raw data residuals for the Mars calibration sequence I pictures are shown in Fig. 12. The expanded time scale facilitates the identification of attitude control limit cycle motion of the spacecraft with a period of about 1.2 hr. This residual limit cycle motion may be due to scale factor errors in the attitude control model. These were, however, not separately included in the estimation but were absorbed in the pointing errors.

The orbit determination (OD) accuracies (Fig. 13) indicate a slow reduction of the SMAA and SMIA with time up to about E-50 hr. Rapid reduction in uncertainty occurs thereafter. At the end of POS II the SMAA is about 70 km, while at the end of POS III it is about 30 km. The time of flight uncertainty shows little improvement, as would be anticipated from our discussion of the approach trajectory.

The Mariner IX optical navigation performance was considerably better than that of Mariner VI and VII.[1] The *B*-plane accuracy was better by a factor of two, while the estimate of

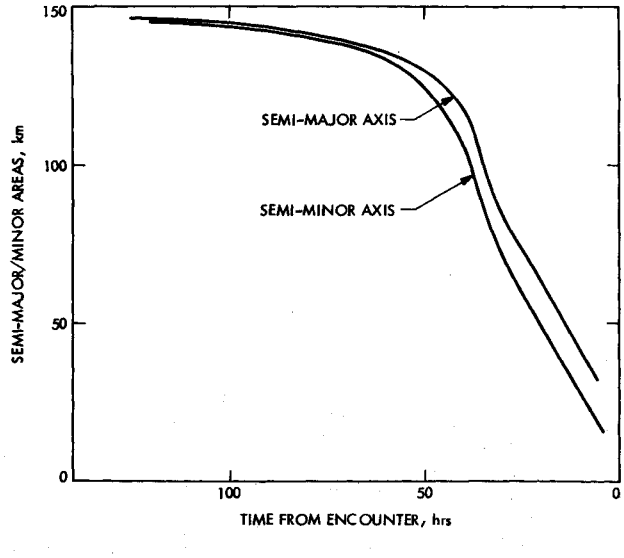

Fig. 13 Expected trajectory estimation accuracy.

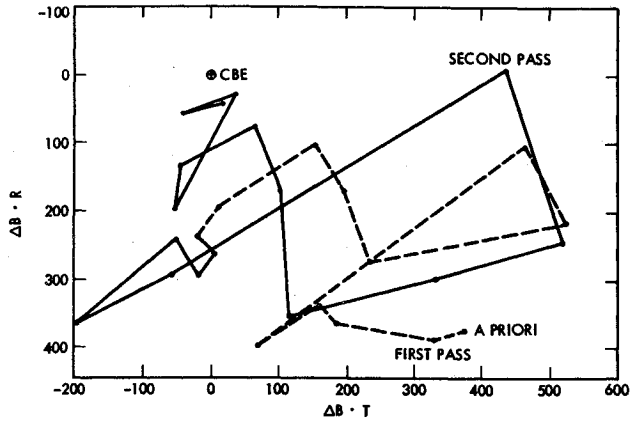

Fig. 14 Sensitivity to Mars ephemeris error.

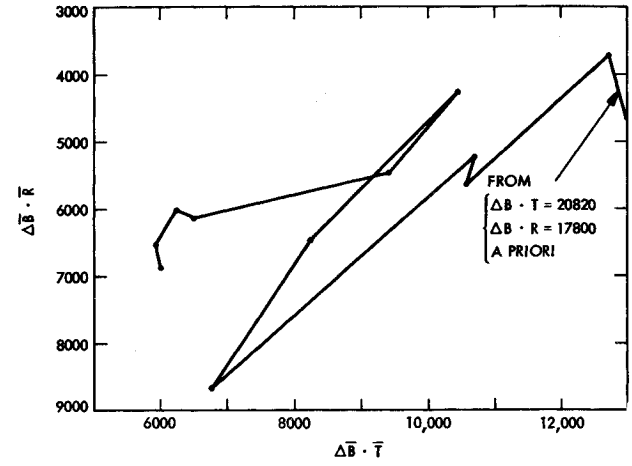

Fig. 16 Optical data solution from injection.

the simulated real-time trajectory solution was a factor of four better. TV pointing was the major source of error.

Sensitivity to Mars Ephemeris

Planetary ephemeris constitutes a major source of error in navigation estimates obtained using radio tracking by stations on Earth.[10] However, from onboard optical data the spacecraft state is directly related to the target planet. To study the effect of Mars ephemeris on the spacecraft trajectory estimate using limb data in conjunction with radio data, a heliocentric error of about 500 km in the orbit of Mars was introduced. The *B*-plane solution history (Fig. 14) shows that the first pass through the data moves the estimate by 300 km from the a priori, which is more than 500 km from the CBE (origin). The final iteration moves the estimate to within 40 km of the CBE. The relative insensitivity of optical data to Mars ephemeris errors makes combined radio and optical solutions an attractive mode of navigation.

Sensitivity to Radio Tracking

As indicated before, optical data suffer a serious limitation in that an accurate determination of the time of flight and V_∞ is not obtained. However, for the Mariner IX trajectory geometry these are precisely the parameters that can be accurately determined from the radio data. To give better estimates of encounter conditions much earlier than either data separately could, a combination of optical and radio data then, would be ideal. Two different analyses were carried out to study the reliance of optical limb data solutions on a priori obtained from the radio data arcs. In the first, a few hours of radio tracking was assumed beyond the first midcourse maneuver at launch (L)+5 days, and no more radio data thereafter. The spacecraft state estimate and covariance at that time were input as a priori to the optical data arc. The mapped *B*-plane uncertainties were very large at this point owing to large maneuver execution uncertainties being mapped several months forward. The analysis was conducted using only the TV pictures through POS II—that is, pictures that could have been used for a real-time "optical only" solution before computing the Mars orbit insertion maneuver.

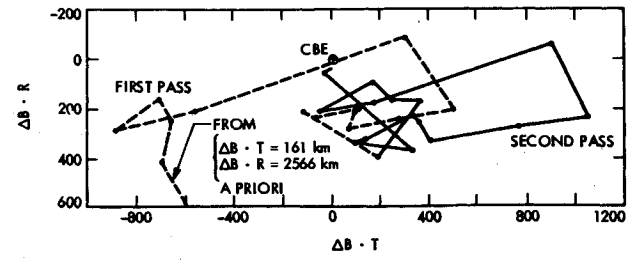

Fig. 15 Optical data solution from midcourse maneuver.

The *B*-plane solution is shown in Fig. 15. The a priori was more than 2500 km from the CBE in the *B*-plane. The first pass moved the estimate at the end of POS II to within 450 km of the CBE. The next pass did not appreciably move the POS II solution, but the POS III data moved the estimate to within 30 km. This accuracy is within mission requirements for inserting the Mariner IX into orbit.

The second analysis was performed with no radio data at all. The injection conditions, for purposes of planetary quarantine (PQ), had a 25,000 km aim-point bias and 22 hr lag in time of flight at Mars. The analysis made here for this optical-only solution was not cognizant of the midcourse maneuver performed at L+5 days which removed the PQ bias. The *B*-plane trajectory solution (Fig. 16) stabilized at about 7000 km from the CBE, with negligible improvement in time of flight.

The large final error involved here indicates that for optimum results, both radio and optical limb data types are necessary. Even small radio data arcs, when used to give a priori estimates and covariances, improve the effectiveness of optical limb-data enormously (Fig. 15).

Conclusions

It has been successfully demonstrated that the TV pictures of Mars on the MM'71 mission were a good source of navigational data. The inflight calibration of the scan platform, performed by referencing star images in TV pictures, significantly improved the onboard optical data accuracy. Inflight TV camera calibration resulted in the accuracy of 0.7 (1σ) and 0.5 (1σ) in pixel and line directions, respectively. The image of Mars observed through TV cameras was found to be a function of a light-scattering surface in the Martian atmosphere rather than the Mars surface. A simple limb fit algorithm yielded sufficient accuracy ($\sim$30 km 1σ) to estimate the center location of Mars.

The Mars limb data combined with radio data gave a *B*-plane estimate within 25 km of the current best estimate, with an uncertainty of 70 km. The addition of Mars limb data to radio data reduces sensitivity to planetary ephemeris errors, nongravitational spacecraft acceleration errors, and Earth-based tracking station location errors. The limb data was found to be somewhat sensitive to the amount of radio data used but not to Mars

ephemeris errors. A combination of optical and radio data yields the best results, and much earlier than either data can separately.

Results from Mariner IX were a factor of four better than those from the Mariner VI and VII missions. This can be attributed primarily to better TV pointing estimation owing to the inflight calibration performed. Despite this, the major source of error was still found to be the TV pointing. For future missions significant improvement in navigation using limb data would result from two TV cameras wherein one of them would be used for imaging stars to determine TV camera pointing.

References

[1] Duxbury, T. C. and Breckenridge, W. G., "Mariner Mars 1969 Optical Approach Navigation," AIAA Paper 70-70, New York, 1970.

[2] Duxbury, T. C., Born, G. H., and Jerath, N., "Viewing Phobos and Deimos for Navigating Mariner 9," *Journal of Spacecraft and Rockets*. Vol. 11, No. 4, April 1974, pp. 215–222.

[3] Jerath, N., "Evaluation of Optical Data for Mars Approach Navigation," presented at the Institute of Navigation Annual Meeting, West Point, N.Y., June 27–29, 1972.

[4] Duxbury, T. C. and Ohtakay, H., "In-flight Calibration of an Inter Planetary Navigation Instrument," *Journal of Spacecraft and Rockets*, Vol. 8, No. 10, Oct. 1971, pp. 1038–1042.

[5] Ohtakay, H. and Jerath, N., "Mariner Mars '71 Optical Lit Limb Data Measuring Techniques and Navigation Results," AIAA Paper 73-251, Washington, D.C., 1973.

[6] Breckenridge, W. G. and Acton, C. H., Jr., "A Detailed Analysis of Mariner IX TV Navigation Data," AIAA Paper 72-866, Palo Alto, Calif., 1972.

[7] Duxbury, T. C., "Navigation Data from Mariner Mars 1969 TV Pictures," *Navigation*, Vol. 17, No. 3, Fall 1970, pp. 219–225.

[8] Cain, D. L. et al., "Approximations to the Mean Surface of Mars and Mars Atmosphere using Mariner 9 Occultations," *Journal of Geo-Physical Research*, Vol. 78, No. 20, 1973, pp. 4352–4354.

[9] Wong, S. K., private communications, April 3, 1973, Jet Propulsion Lab., Pasadena, Calif.

[10] Jordan, J. F., Madrid, G. A., and Pease, G. E., "Effects of Major Error Sources on Planetary Spacecraft Navigation Accuracies," *Journal of Spacecraft and Rockets*, Vol. 9, No. 3, March 1972, pp. 196–204.